IET Generation, Transmission & Distribution

Research Article

IET Journals
The Institution of Engineering and Technology

Mitigation of switching overvoltages in microgrids based on SVC and supercapacitor

ISSN 1751-8687
Received on 30th March 2017
Revised 11th August 2017
Accepted on 27th August 2017
E-First on 30th October 2017
doi: 10.1049/iet-gtd.2017.0503
www.ietdl.org

Eman A. Awad[1], Ebrahim A. Badran[1] ✉, Fathi H. Youssef[1]

[1]*Electric Engineering Department, Faculty of Engineering, Mansoura University, Mansoura, Dakahlia Governorate 35516, Egypt*
✉ *E-mail: ebadran@mans.edu.eg*

Abstract: This study investigates three different techniques to mitigate the switching overvoltages (SOVs) in the microgrids. At first, the effectiveness of reactive power compensation devices, such as static var compensator (SVC), is evaluated. After that, the performance of the supercapacitor (SC), as an energy storage device, is studied. Finally, with the addition of the SVC to the SC, the possibility to mitigate SOV by compensating both active and reactive power simultaneously is investigated. SOVs result due to unsymmetrical switching operation during de-energisation (disconnection) procedures. The μG two operational modes; grid connected mode and isolated mode, are considered. A small hydro generation unit and three variable speed, double-fed induction generator-based wind turbines are the main renewable power generation units in the tested microgrid system. Alternative Transient Program is used in this study for simulating the compensation device, the energy storage device and the investigated microgrid. The study shows that through the μG two operational modes, the SC has priority over the other two investigated mitigation methods. Furthermore, using the SC or SC with SVC, the results have more regular voltage waveforms.

1 Introduction

Switching overvoltages (SOVs) are considered the most severe type of overvoltage originated on the power systems [1–2]. SOVs are known to have low front transient, which are highly damped, and last for a short duration (few milliseconds or less) [3–5]. Switching events and system disturbances lead to the energy exchanges subject the circuit components to higher stresses, resulting from excessive currents or voltage variations. The switching procedures can cause high overvoltage stresses mainly along the transmission line but also in the supply network [6]. A stuck pole on a circuit breaker (open or closed) can result in SOVs that produce a voltage several times normal magnitude on the open phases [7]. A traditional method of limiting SOVs to acceptable levels is to use circuit breakers equipped with pre-insertion resistors, circuit breakers controlled switching, shunt reactors, and surge arresters [4].

Var compensation is defined as the management of reactive power to improve the performance of ac power systems [8, 9]. Switching and temporary overvoltage limitation, optimisation of reactive power flow, voltage control, reduction of system losses, and power factor adjustment are some of Var compensation benefits [10, 11].

Static Var Compensators (SVCs) are the most popular first generation shunt device belongs to flexible AC transmission systems. Mainly, SVC consists of a fast thyristor switch controlling a shunt capacitor or inductor which improves voltage and stability. The variation of reactive power is performed by switching three-phase capacitor banks and/or inductor banks connected on the secondary side of a coupling transformer. Reactors are either switched on-off as thyristor switched reactor or phase-controlled as thyristor controlled reactor (TCR) [9, 12–17].

Supercapacitors (SCs), also known as ultracapacitors or electric double-layer capacitors, are finding use in a variety of power management applications [18–22]. SCs are usually low voltage, high capacity devices with milliohm order equivalent series resistances. They usually have time constants from fractional seconds to seconds. Due to these long time constants, compared to the time durations of power line transients in the range of few microseconds to several hundred microseconds, these devices may be able to withstand short duration surges [23].

During the last decade, there have been many attempts to measure the commonly used technical parameters to characterise the SC behaviour. These literature introduce the installation of SC in the transmission power system as for a new method to reduce transient overvoltages [22, 24]. However, a few of this literature has attempted to characterise SCs effect on SOVs that last milliseconds [19–23].

The American department of energy (DOE) defines the microgrid (μG) as 'a group of interconnected loads and distributed energy resources within clearly defined electrical boundaries that act as a single controllable entity with respect to the grid.' μGs have been identified as a key component of the Smart Grid for improving power reliability and quality, increasing system energy efficiency, and providing the possibility of grid-independence to individual end-user sites [25, 26]. A μG can operate in parallel to the grid (grid-connected mode) or islanded mode and hence increases the reliability of energy supplies by disconnecting from the grid in the case of network faults or reduced power quality [27].

In this paper, the effectiveness of reactive power compensation devices, such as SVC, is evaluated in Section 2. Also, the performance of a proposed SC, as energy storage device and a SOV mitigation method, is studied. Then in Section 3, the tested microgrid system is described and Alternative Transient Program (ATP) is used for simulating the SVC model, the proposed SC-based mitigation method model, and the investigated μG system. Finally, in Section 4, mitigation of SOV in μG based on SVC and/or SC are investigated. SOVs result due to unsymmetrical switching operation during the de-energisation procedures. Separately, the μG two operational modes, grid connected mode and isolated mode, are considered.

2 Description and modelling of the SOV mitigation methods

2.1 SVC-based SOV mitigation method

The SVC-based SOV mitigation method considered, in this paper, will deal with SVC that consists of a TCR in parallel with a fixed capacitor (FC). TCR is one of the most important building blocks of thyristor-based SVCs [28, 29].

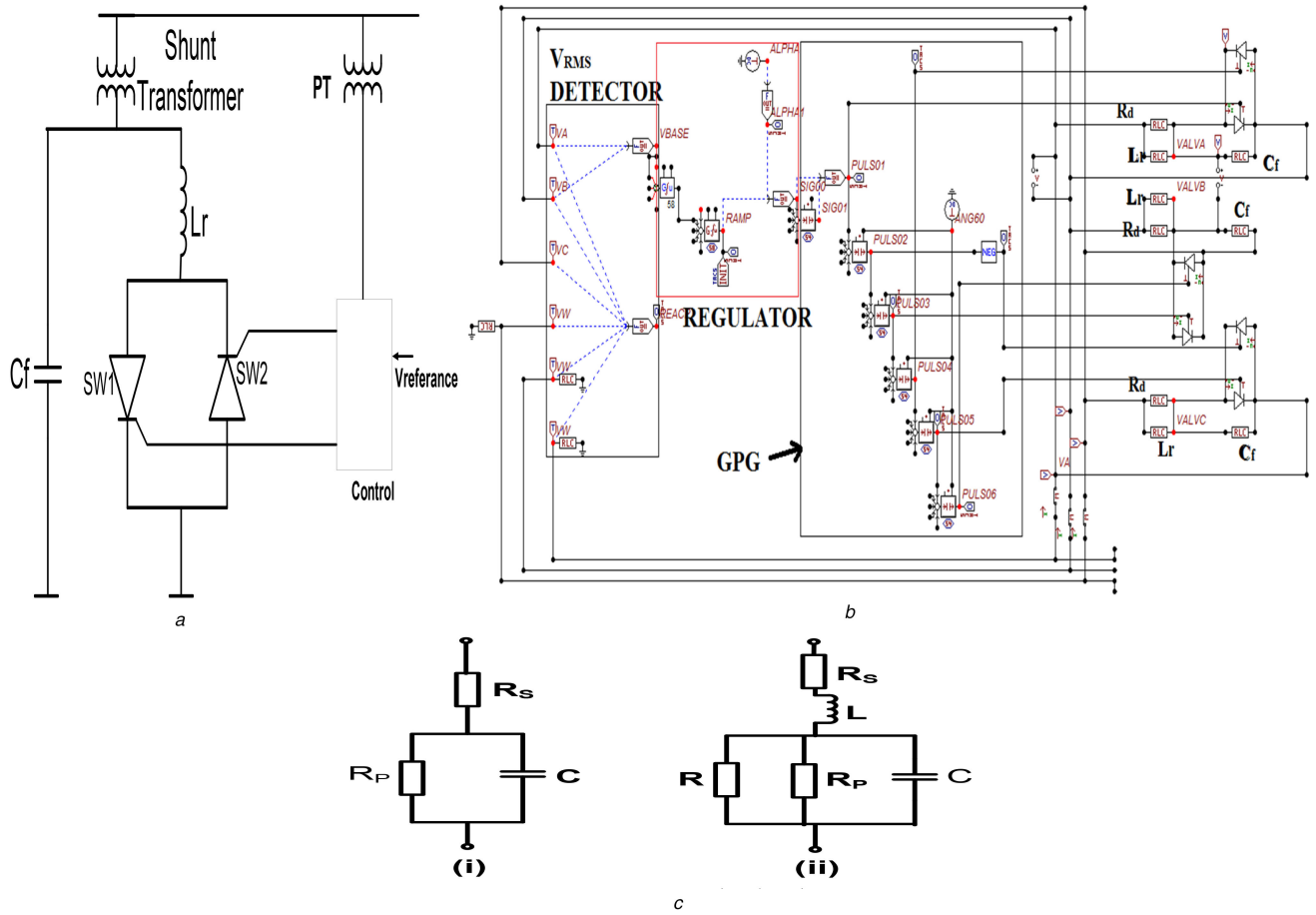

Fig. 1 *Studied SOV mitigation methods, SC and SVC*
(a) SVC single-line diagram ***(b)*** SVC model in ATP ***(c)*** Equivalent circuit of SC (i) classical, (ii) proposed

In the SVC model, the switching elements are two oppositely poled thyristors which conducted on alternate half cycles of the μG generation units' frequency [29, 30].

The inductor (L_r) which is connected in series with the thyristors, in the TCR, is given by

$$\frac{1}{L_r} = \frac{\omega P}{V_{rms}^2}\left(\frac{P}{Q} + \frac{Q}{P}\right) \tag{1}$$

where ω is the angular frequency, P is the rated TCR active power, V_{rms}^2 is the RMS voltage of the TCR, and Q is the rated TCR reactive power.

For the continuity of the TCR, as the reactor current is not continuous, thyristors controlled inductors are installed between phases in delta connection [29].

The capacitive reactance (X_C) of the FC (C_f) connected in parallel with the TCR is given by

$$X_C = \frac{V_{rms}^2}{Q} \tag{2}$$

A damping resistor (R_d) is introduced, in this study, across the inductor (L_r) to stop the problem of numerical oscillation. This reactor is represented as

$$R_d = \frac{L_r}{\beta\,\Delta t} \tag{3}$$

where β is a damping factor of the reactor, $0 \le \beta \le 1$, and Δt is the time step of the simulation.

The control system of the TCR model consists of three parts; the gate pulse generator (GPG), the regulator, and the RMS voltage detector. GPG provides the firing pulses to the thyristors. The regulator calculates the conduction angle, which is passed to the GPG as a control signal. Finally, the RMS voltage detector interfaces the TCR with the μG system. In this case, TCR measures the RMS voltage [29]. Fig. 1*a* shows the simulation of the SVC model in ATP.

2.2 Proposed SC-based SOV mitigation method

There are many models and equivalent circuits introduced in the literature for SC [31, 32]. The electrical equivalent circuit of the proposed SC-based mitigation method is illustrated in Fig. 1*b*. The parameters of the proposed SC-based mitigation method include equivalent series resistance (R_S), small reactor (L), equivalent parallel resistance (R_P), and capacitance (C).

R_S is usually put forward to describe internal resistance when the SC is estimated. The voltage during discharge is determined by R_S [33, 34]. R_S wastes power for internal heating when charging or discharging in the SCs. R_S is almost in the range of 100 mΩ–10 Ω but influences the energy efficiency and power density [22, 33]. The equivalent series resistance (R_S) for the proposed SC-based mitigation method is given by

$$R_S = \frac{V_C^2}{4 \times P_{max}} \tag{4}$$

where R_S is the equivalent series resistance of the SC bank in ohm, V_C is a maximum voltage of the SC bank in volts, and P_{max} is maximum dischargeable power in VA [34].

As shown in Fig. 2, a small reactor (L) is added is in series with the series resistances R_S. The reactor with the help of R_S will perform a useful high-pass filter function to reduce the harmonics in the waveform and make it smoother.

R_P is an inner equivalent parallel resistance usually in the order of several kilo-ohms and decides the leakage current when the proposed SC is in a standby mode [33, 35].

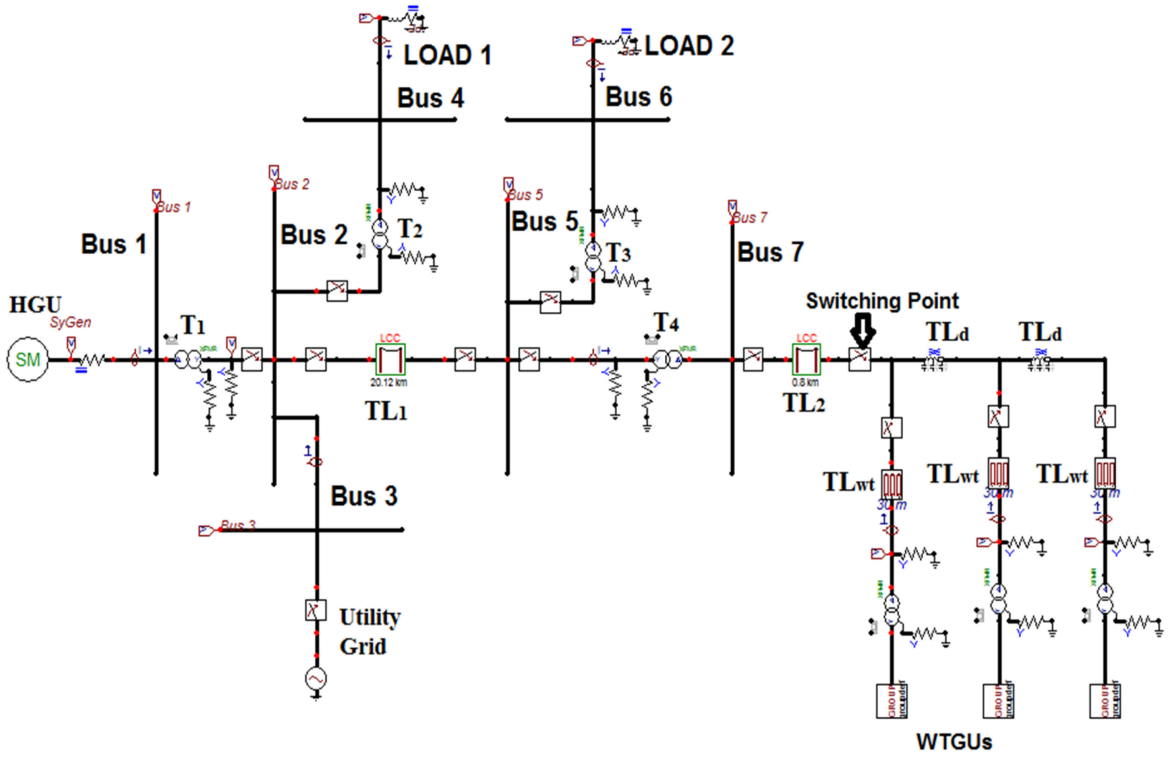

Fig. 2 *Microgrid test system model in ATP*

Table 1 Parameters of the DFIG-based WT

stator resistance	0.0025 Ω
stator leakage inductance	0.097 mH
magnetisation inductance	3 mH
rotor resistance	0.0383 Ω
rotor leakage inductance	0.115 mH
electrical turn ratio	4
moment of inertia (inertia constant = 2 s)	2.400 kg m^2
rated apparent power	6.500 kVA

R is an equivalent resistance result from adding a resistance R_E in parallel with R_P. The equivalent resistance R_E is defined by

$$R_E = \frac{V_c}{I_D} \tag{5}$$

The capacitance C of the proposed SC-based mitigation method in μF can be expressed on the assumption that, if a single step voltage of V_{max} in volts and time duration of T in seconds is applied to the SC, the approximate final voltage developed at the capacitor is given by

$$V_c = \frac{T}{R_S \times C} V_{max} \tag{6}$$

Equation (6) provides that the surge duration T is very much shorter than the time constant of the circuit $\mathbf{T} = R_S C$ [22].

The proposed SC design is simple and there is no need for non-linear devices. The proposed SC-based mitigation method is designed to absorb SOVs superimposed on the mains utility AC supply.

3 Description and modelling of the tested microgrid system

3.1 Description of the tested microgrid system

Fig. 2 shows the investigated μG test system model in ATP. The μG system consists of two DG systems, the first DG system consists of a single hydro generation unit (HGU) which is connected to bus 1 using a 6.9/66 kV, 8 MVA power transformer. The second DG system is a wind power generation system (WPGS) which consists of three wind turbines (WTs). Each turbine is connected to a 0.69/12.5 kV, 5 MVA power transformer. The three turbines are separated from each other by a 30 m transmission line TL_d. The second DG system is connected to bus 7 through an 800 m transmission line TL_2 and a 12.5/66 kV, 45 MVA power transformer. The utility grid is represented by a 66 kV, 1000 MVA grid connected to bus 3. There are two load areas represented as Load-I and Load-II. Load-I is connected to bus 4 and the power is delivered to the load using a 66/12.5 kV, 5 MVA power transformer. Load-II is connected to bus 6 and the power is delivered to the load using a 66/12.5 kV, 4 MVA power transformer. The two load areas are connected to the two generating systems by a 20.12 km transmission line TL_1 [36, 37].

3.2 Modelling of wind power generation unit

The WPGS model consists of three variable speed doubly-fed induction generators (DFIGs)-based WTs. DFIG is one of the most commonly used technologies for wind generation purposes nowadays [38, 39]. A complete WT model includes the wind speed model, the aerodynamic model of the WT, and models of the electrical components, is used in this study [38]. Table 1 summarises the data used to parameterise the DFIG-based WT model used in ATP.

3.3 Modelling of hydro power generation unit

A conventional synchronous generator is used for the HGU. The synchronous generator is modelled in a d–q rotor reference frame with the dynamics of stator, rotor and damper windings [37]. Synchronous generator parameters are obtained from [40]. The synchronous generator model data in ATP are listed in Table 2.

3.4 Modelling of transformers

The transformers of the μG are modelled using three phases, two windings model. Table 3 gives the simulation data of the transformers. All the transformers at μG system are modelled using the hybrid transformer model XFMR. The XFMR model is suitable for low and medium frequency transient studies [41, 42].

3.5 Modelling of overhead lines

Three-phase 12.5 kV overhead lines, that connect between the two load areas and the generation units, are modelled using the frequency dependent (line/cable constant) model. This model represents the frequency dependence of overhead lines parameters; so this model is much recommended for the electromagnetic transient studies [43].

The overhead lines have two conductors in a bundle: cross-sectional area of 2×670 mm^2, three-phase, with skin effect, segmented grounding and transposition are considered in the modelling, the ground resistivity is 120 Ωm. The parameters and location of the conductors on the tower are given in Table 4 [44].

Table 2 Parameters of the synchronous generator-based HGU

S_n = 5 MVA	x_0 = 0.046 pu
U_n = 6.6 kV	T'_{d0} = 1.754 s
R_A = 0.004 pu	T'_{q0} = 0 s
x_L = 0.1 pu	T'_{d0} = 0.019 s
x_d = 1.8 pu	T'_{q0} = 0.164 s
x_q = 1.793 pu	H = 74.8 kg m^2
x'_d = 0.166 pu	P = 4 poles
x'_q = 0.98 pu	f = 60 Hz
x'_d = 0.119 pu	ω_s = 188.5 rad/s
x'_q = 0.17 pu	—

Table 3 Microgrid's transformers data

Data	T1	T2	T3	T4	Twt
connection method	Y_Nd_{11}	Y_Nd_{11}	Y_Nd_{11}	Y_Nd_{11}	Y_Nd_{11}
voltage, kV	6.9/66	66/12.5	66/12.5	66/12.5	0.69/12.5
rated power, MVA	10	5	4	30	5
S.C Imp*, %	9	8	8	9	5.7
copper losses, kW	24.75	32.4	28.8	126.9	1.58
no-load losses, kW	11.2	7.2	6.08	31.8	0.97
no-load current, %	0.9	1	1.1	0 6	0.9

S.C Imp*: short-circuit impedance.

Table 4 Parameters of the 12.5 kV transmission lines

phase no	1	2	3	0
R_{in}, cm	0.63	0.63	0.63	0
R_{out}, cm	1.81	1.81	1.81	0.5
Resis, Ω/km	0.042	0.042	0.042	0.2
Horiz, m	−2	0	2	0
V_{tower}, m	14	14	14	18
V_{mid}, m	11	11	11	15
Separ, cm	40	40	40	0
Alpha, deg.	0	0	0	0
NB	0	2	2	1

Table 5 SVC-based mitigation method model data

Parameters	L_r	C_f	R_d
values	34 mH	10 μF	100 Ω

Table 6 Proposed SC-based mitigation method model data

Parameters	C	R_S	R_E	L
Values	6.9 μF	1.44 Ω	2.8 Ω	1.74 mH

3.6 Modelling of SOVs mitigation methods

SVC model is given in Fig. 1 is connected nearby the switching point. The parameters of SVC model, for each phase, are calculated by (1)–(3). These parameters are given in Table 5.

The proposed SC-based mitigation method is connected nearby the switching point. The parameters of the proposed SC-based mitigation method model are calculated by (4)–(6). These parameters are given in Table 6.

4 Mitigation of SOV in microgrid based on SVC and/or SC

The mitigation of SOV is proposed, in this paper, using reactive power compensation devices, such as SVC, and an energy storage device, such as SC. The effectiveness of SVC and/or the SC, separately and simultaneously, as SOV mitigation methods are studied. The SOVs due to unsymmetrical switching operation during a faulty WT generation units (WTGUs) de-energisation (disconnection) operation on a μG system is studied. Two different scenarios are taken into consideration in this investigation. The μG two operational modes, grid connected mode and isolated mode, are taken into consideration in this study. In the μG two operational modes, the unsymmetrical switching is carried out by the de-energisation of both phases B and C of the switching circuit breaker. Fig. 2 illustrates the switching point in the system, where it is located nearby WTGUs.

The unsymmetrical switching operations are applied at $t = 0.03$ s. This time is chosen because at this moment the voltages at phases B and C reach 85% of their maximum values together, and thus the worst expected case of the de-energisation. The timeline of the switching operation on the μG two operational modes is listed below:

A.Grid connected mode

i. At $t = 0.03$ s, switching operations are applied.
ii. At $t = 0.03$ s, disconnected phases B and C but phase A still connected.
iii. Overvoltage occurs.

B. Isolation mode

i. At $t = 0.015$ s, the μG is isolated from the grid.
ii. At $t = 0.03$ s, switching operations are applied.
iii. At $t = 0.03$ s, disconnected phases B and C but phase A still connected.
iv. Overvoltage occurs.

4.1 Grid connected mode

The μG is connected to the grid when the SVC and/or the SC are installed. Fig. 3 shows the effect of using the mitigation methods on maximum SOVs at the first WT output, and the active and reactive power injected by the same WT into the microgrid, respectively.

Due to using the SVC, the maximum SOV at the first WT is reduced from 4.28 (2.954) to 1.162 pu (0.802 kV). However, due to using the SC, the maximum SOV at the first WT is reduced from 4.28 (2.954) to 1.041 pu (0.718 kV). While, due to using both the SVC with the SC, the maximum SOV at the first WT is reduced from 4.28 (2.954) to 1.138 pu (0.785 kV).

It can be noticed that, as a SOV mitigation method, the SC has priority over the other two investigated mitigation methods. Using the SC or the SC with the SVC results in more regular voltage waveform comparing with using only the SVC.

It can be seen that all the investigated mitigation methods increase the active power injected by the first WT into the grid. However, using the SC or the SC with the SVC enhances the performance of the WT by increasing its injected active power into the grid to values close to WT steady-state value.

The reactive power injected by the first WT increases to a higher value than its steady-state value using the SVC or the SC

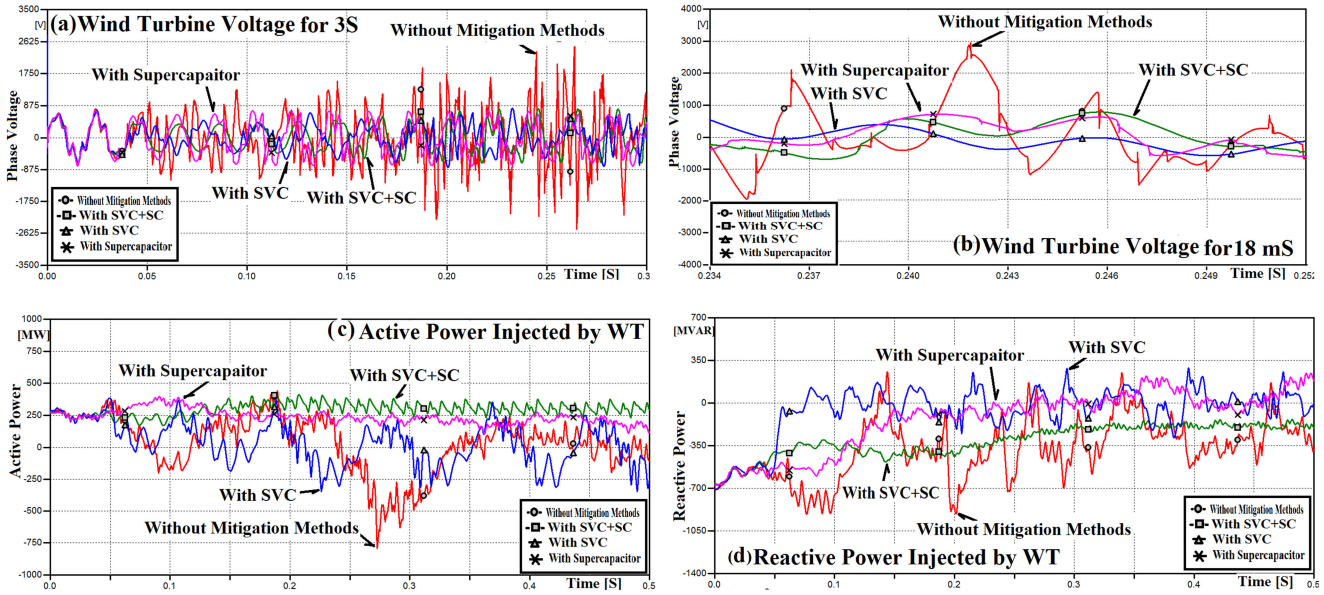

Fig. 3 *Effect of SOV at the first WT with and without mitigation methods*

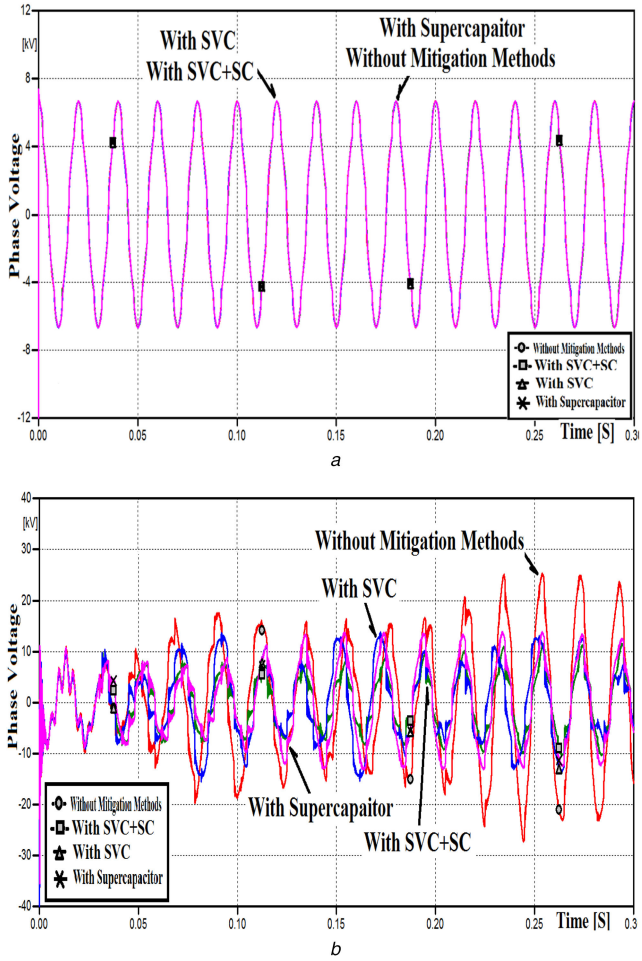

Fig. 4 *Maximum SOV at*
(a) Bus 1 and ***(b)*** Bus 7 output voltage with and without mitigation methods

separately. While, by adding the SC to the SVC, the reactive power reaches value more stable and closes to WT steady-state value.

Fig. 4 shows the maximum SOVs at Buses 1 and 7 respectively, with and without using the investigated mitigation methods.

Bus 1 is connected to HGU directly, so Bus 1 output voltage also represents HGU output voltage. Bus 1, the furthest busbar to the switching point, is not affected by adding any of the investigated mitigation methods to the μG system.

By using the SVC, the maximum SOV at Bus 7 is reduced from 3.8 (27.353) to 2.163 pu (15.57 kV). However, due to using the SC, the maximum SOV at Bus 7, the nearest busbar to the switching point, is reduced from 3.8 (27.353) to 1.93 pu (13.87 kV). While due to using the SVC with the SC, the maximum SOV at the first WT is reduced from 3.8 (27.353) to 1.6 pu (11.478 kV).

It can be noticed that the SC with the SVC, as a SOV mitigation method, has priority over the other two investigated mitigation methods. Bus 7 voltage waveforms become more regular due to using the SC or SC with SVC comparing with using the SVC only.

Fig. 5 illustrates the harmonic analysis of the maximum SOVs generated at Bus 7 without mitigation and with the SVC and/or the SC, separately and simultaneously, respectively.

It can be seen that with the SVC the voltage waveform is smoother which means fewer harmonics in the waveform comparing with the SC or SC with SVC.

The output voltage of Load-I and Load-II appears to be not affected by using the SVC or the SC-based mitigation methods.

4.2 Isolated mode

The μG in isolated mode is investigated when the SVC and/or the SC is installed. The μG is isolated from the grid at $t = 0.015$ s.

Fig. 6 shows the maximum SOVs at the first WT, and the active and reactive power injected by the same WT, respectively, with and without using the investigated mitigation methods.

Due to using the SVC, the maximum SOV at the first WT is reduced from 4.94 (3.41) to 1.38 pu (0.952 kV). However, due to using the SC, the maximum SOV at the first WT is reduced from 4.94 (3.41) to 1.021 pu (0.704 kV). While, due to using the SVC with the SC, the maximum SOV at the first WT is reduced from 4.94 (3.41) to 1.35 pu (0.93 kV).

It can be noticed that, as a SOV mitigation method, the SC has priority over the other two investigated mitigation methods. Using the SC or SC with SVC results in more regular voltage waveform comparing with using the SVC only.

It can be seen that using the SC or the SC with the SVC, enhances the performance of the WT by increasing its injected active power into the grid.

Using SVC separately or by adding the SC with the SVC, increase the reactive power injected by the first WT to a higher value than its steady-state value. While due to using the SC separately the reactive power injected by the first WT decrease to values below its steady-state value.

Fig. 7 shows the effect of using the investigated mitigation methods on the maximum SOVs at Buses 1 and 7, and the maximum SOVs at Load-I and Load-II, respectively.

It appears that by using the mitigation methods, there is a slight increase in Bus 1 voltage after its decrease as a result of the

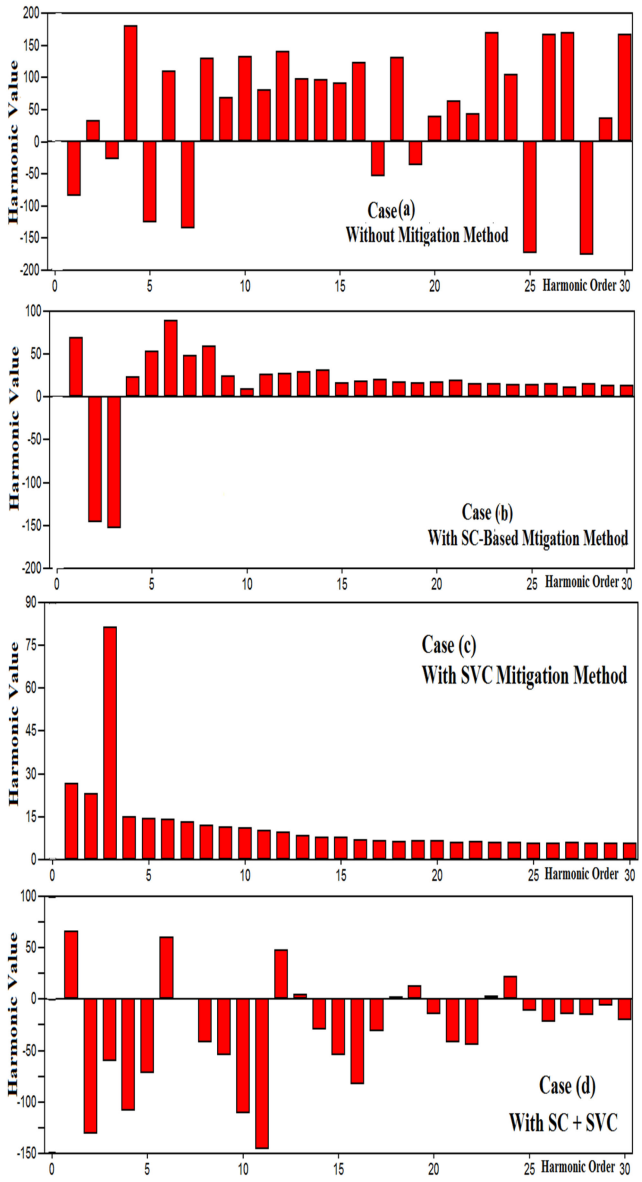

Fig. 5 *Harmonic analysis of the SOVs at Bus 7*

switching operation. However, SVC separately seems to be more effective in overcoming SOV due to the isolation process comparing with the other two investigated mitigation methods.

By using the SVC, the maximum SOV at Bus 7 is reduced from 2.316 (16.674) to 1.14 pu (8.208 kV). However, due to using the SC, the maximum SOV at Bus 7, the nearest busbar to the switching point, is reduced from 2.316 (16.674) to 1.023 pu (7.366 kV). Due to using the SVC with the SC, the maximum SOV at the first WT is reduced from 2.316 (16.674) to 0.96 pu (6.902 kV).

Bus 7 voltage waveforms become more regular due to using the SC or the SC with the SVC comparing with using the SVC only. It can be noticed that adding the SC with the SVC, has priority over the other two investigated SOV mitigation methods.

The reduction by using the investigated mitigation methods, at Load-I and Load-II, is not considered effective. However, the SVC separately seems to be more effective in overcoming SOV due to the isolation process comparing with the other two investigated mitigation methods. The investigated mitigation methods are not succeeding to increase the voltage to its steady-state values, after its decrease as a result of the switching operation. Table 7 summarises the investigated mitigation methods effect on the μG during the two operational modes.

4.3 Other switching scenarios

Other switching scenarios such as disconnecting one of the WT generation units, as there is insufficient wind resource to produce electricity are also modelled. Table 8 summarises the tested mitigation methods effect on the μG during the two operational modes in the two investigated switching scenarios.

It can be seen that using the SC or the SC with the SVC has priority over the other two investigated SOV mitigation methods at the first WT output voltage and the nearest busbar to the switching point.

5 Conclusion

In this paper, the effectiveness of the SVC and/or the SC as SOV mitigation method is evaluated. To do so the effect of SOVs results for a de-energisation operation on a μG system consisting of renewable power sources is investigated. The μG two operational modes, grid connected mode and isolated mode, are considered. The investigated μG system consists of small HGU and three variables – speed, DFIG-based WTs, and two load areas.

At the first WT output voltage and the nearest busbar to the switching point, the results show that in the μG two operational modes, as a SOV mitigation method, the SC has priority over the other two investigated mitigation methods. However, using the SC

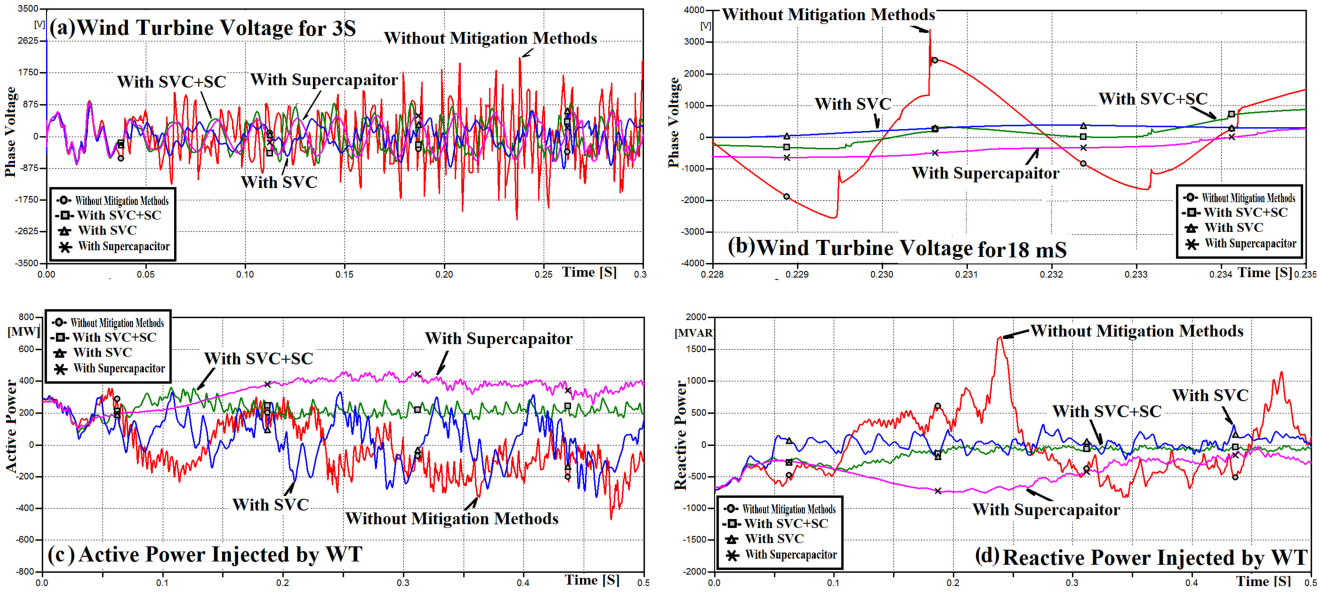

Fig. 6 *Effect of SOV at the first WT with and without mitigation methods (isolated mode)*

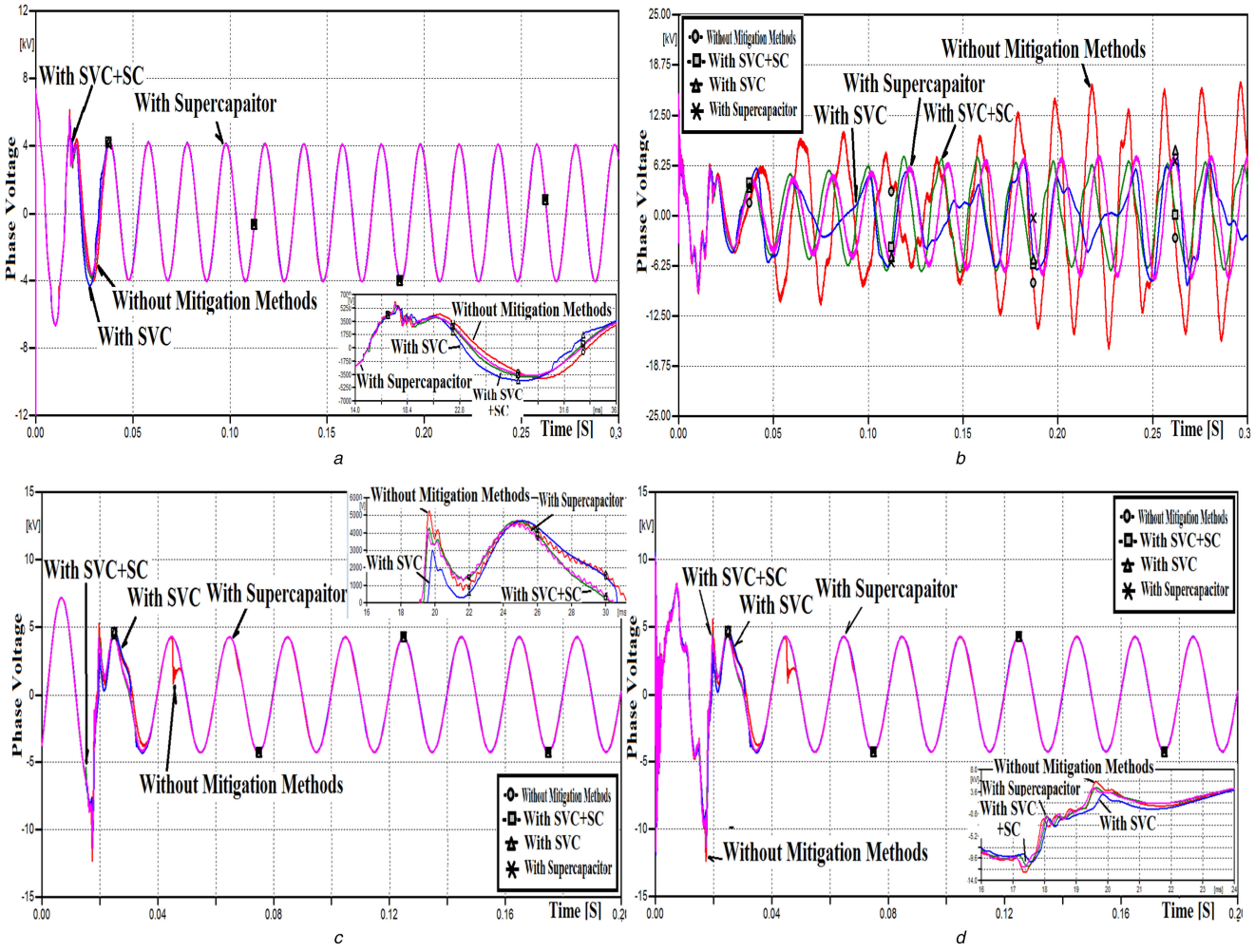

Fig. 7 *Maximum SOV at*
(a) Bus 1, ***(b)*** Bus 7, ***(c)*** Load-I and ***(d)*** Load-II with and without mitigation methods

Table 7 Investigated mitigation methods effect on the μG two operational modes

		Without mitigation methods	SVC	SC	SVC + SC
grid connected mode	WT output voltage, kV	2.954	0.802	0.718	0.785
	Bus 7, kV	27.353	15.57	13.87	11.478
isolated mode	WT output voltage, kV	3.41	0.952	0.704	0.93
	Bus 7, kV	16.674	8.208	7.366	6.902

Table 8 Investigated mitigation methods effect on the μG when WT no. 3 is disconnected

Disconnecting one of the WT generation units (WT3)		Without mitigation methods	SVC	SC	SVC + SC
grid connected mode	WT output voltage, kV	2.305	0.786	0.483	0.487
	Bus 7, kV	23.712	19.307	12.991	12.78
isolated mode	WT output voltage, kV	2.512	0.601	0.48	0.388
	Bus 7, kV	22.22	7.47	6.5	6.204

or the SC with the SVC results in more regular voltage waveform comparing with using the SVC separately.

It can be seen that, in the μG two operational modes, using all the investigated mitigation methods increase the active power injected by the first WT into the grid. However, using the SC or the SC with the SVC enhances the performance of the WT by increasing its injected active power into the grid to values close to WT steady-state value. While, in the μG two operational modes, due to adding the SC with the SVC, reactive power reaches value more stable and closes to WT steady-state value.

However, at the loads, the mitigation methods are not succeeding to raise the voltage to its steady-state values, after its decrease as a result of the switching operation, during the μG two operational modes.

6 References

[1] Shafy, A.S., Emam, A.M., Ghania, S.M., *et al.*: 'Analysis and mitigation techniques of switching overvoltages for a 500 kV transmission line', *Int. Electr. Eng. J., IEEJ*, 2016, **7**, (3), pp. 2196–2203

[2] Soloot, A., Gholami, A., Agheb, E., *et al.*: 'Investigation of transmission line overvoltages and their deduction approach', *Int. J. Electr. Comput. Energetic Electron. Commun. Eng.*, 2009, **3**, (5), pp. 1070–1078

[3] G.I.G.R.E. Working Group: 'Switching overvoltage in EHV and UHV systems with special reference to closing and reclosing transmission lines', *Electra*, 1973, **30**, pp. 70–122

[4] Awad, E.A., Badran, E.A., Youssef, F.H.: 'Mitigation of temporary overvoltages in weak grids connected to DFIG-based wind farms', *J. Electr. Syst., JES*, 2014, **10**, (4), pp. 431–444

[5] King, R., Moore, F., Jenkins, N., *et al.*: 'Switching transients in offshore wind farms – impact on the offshore and onshore networks'. Int. Conf. Power Systems Transients, IPST2011, Delft, the Netherlands, 14–17 June 2011

[6] Sood, D.: 'Reduction of switching over voltages in HV transmission line', *Int. J. Sci. Eng. Res.*, 2013, **4**, (6), pp. 64–68
[7] IEEE PES Wind Plant Collector System Design Working Group: 'Wind power plant grounding, overvoltage protection, and insulation coordination'. IEEE Power & Energy Society General Meeting, PES '09, Alberta, Canada, July 2009
[8] Dixon, J., Morán, L., Rodríguez, J., *et al.*: 'Reactive power compensation technologies: state-of-the-art review', *Proc. IEEE*, 2005, **93**, (12), pp. 2144–2164
[9] Shah, G., Kash, A., Saxena, N.: 'Systematic survey for role of reactive power compensating devices in power system', *Int. J. Electr. Instrum. Eng.*, 2013, **3**, (2), pp. 89–94
[10] Chaves, F.S., Vale, M.H.: 'Power system reactive compensation: evaluation of expansion plans taking into account electromagnetic transient restrictions', *Rev. Controle Autom.*, 2009, **20**, (1), pp. 63–71
[11] Hammad, A., Roesle, B.: 'New roles for static VAR compensators in transmission systems', *Brown Boveri Rev.*, 1986, **73**, pp. 314–320
[12] Akwukwaegbu, I.O., Gerald, I.O.: 'Concepts of reactive power control and voltage stability methods in power system network', *Int. Organisation Sci. Res. J. Comput. Eng., IOSR-JCE*, 2013, **11**, (2), pp. 15–25
[13] Vishwakarma, A., Sahu, D.: 'Efficient voltage regulation in three phase AC transmission lines using static VAR compensator', *Int. J. Adv. Res. Electr. Electron. Instrum. Eng., IJAREEIE*, 2013, **2**, (5), pp. 1773–1780
[14] Shea, J. J.: 'Understanding FACTS concepts and technology of flexible AC transmission systems', *IEEE Electr. Insul. Mag.*, 2002, **18**, (1), p. 46
[15] Ambriz-Perez, H., Acha, E., Fuerte-Esquivel, C.: 'Advanced SVC models for Newton–Raphson load flow and newton optimal power flow studies', *IEEE Trans. Power Syst.*, 2000, **15**, (1), pp. 129–136
[16] Porate, K., Thakre, K.: 'Voltage stability enhancement of low voltage radial distribution network using static VAR compensator: a case study', *WSEAS Trans. Power Syst.*, 2009, **4**, (1), pp. 32–41
[17] Fetouh, T., Zaky, M. S., 'New approach to design SVC-based stabiliser using genetic algorithm and rough set theory', *IET Gener. Transm. Distrib.*, 2017, **11**, (2), pp. 372–382
[18] Rufer, A., Barrade, P.: 'A supercapacitor-based energy storage system for elevators with soft commutated interface', *IEEE Trans. Ind. Appl.*, 2002, **38**, (5), pp. 1151–1159
[19] Kakimoto, N., Satoh, H., Takayama, S., *et al.*: 'Ramp-rate control of photovoltaic generator with electric double-layer capacitor', *IEEE Trans. Energy Convers.*, 2009, **24**, (2), pp. 465–473
[20] Belyakov, A. I., Sojref, D. A.: 'High power supercapacitor's solutions for reliable power supply'. Power Engineering Energy and Electrical Drives Conf., POWERENG '09, Lisbon, Portugal, March 2009, pp. 348–352
[21] Zarghami, M., Crow, M. L., Sarangapani, J., *et al.*: 'A novel approach to inter-area oscillation damping by unified power flow controllers utilizing ultracapacitors', *IEEE Trans. Power Syst.*, 2010, **25**, (1), pp. 404–412
[22] Kularatna, N., Fernando, J., Pandey, A., *et al.*: 'Surge capability testing of supercapacitor families using a lightning surge simulator', *IEEE Trans. Ind. Electron.*, 2011, **58**, (10), pp. 4942–4949
[23] Kularatna, N., Fernando, J., Pandey, A.: 'Surge endurance capability testing of supercapacitor families'. IEEE Industrial Electronics Society Conf., IECON 2010, Glendale, USA, November 2010, pp. 1858–1863
[24] Fernando, J., Kularatna, N.: 'Supercapacitor assisted surge absorber (proposed SCASA) technique: selection of supercapacitor and magnetic components'. Energy Conversion Congress and Exposition, ECCE, Pittsburgh, USA, 14–18 September 2014, pp. 1992–1996
[25] Ton, D. T., Smith, M. A.: 'The U.S. department of energy's microgrid initiative', *Electr. J.*, 2012, **25**, (8), pp. 84–94
[26] Mariam, L., Basu, M., Conlon, M.: 'A review of existing microgrid architectures', *J. Eng.*, 2013, **10**, pp. 1–8
[27] Mirsaeidi, S., Said, D., Mustafa1, M., *et al.*: 'Review and analysis of existing protection strategies for micro-grids', *J. Electr. Syst., JES*, 2014, **10**, (1), pp. 1–10
[28] Khonde, S., Palandurkar, M.: 'Simulation model of thyristor controlled reactor', *Int. J. Eng. Res. Technol., IJERT*, 2014, **3**, (4), pp. 1692–1694
[29] TCR Modeling Using ATP, EPRI Report, 1995
[30] Mahapatra, S., Goyal, A., Kapil, N.: 'Thyristor controlled reactor for power factor improvement', *Int. J. Eng. Res. Appl., IJERA*, 2014, **4**, (4), pp. 55–59
[31] Spyker, R. L., Nelms, R. M.: 'Classical equivalent circuit parameters for a double-layer capacitor', *IEEE Trans. Aerosp. Electron. Syst.*, 2000, **30**, (3), pp. 829–836
[32] Hajizadeh, A., Golkar, M. A., Norum, L.: 'Robust control of hybrid fuel cell/energy storage distributed power generation system in weak grid under balanced and unbalanced voltage sag', *Eur. Trans. Electr. Power*, 2011, **21**, (1), pp. 522–540
[33] Sahay, K., Dwivedi, B.: 'Design and analysis of supercapacitor energy storage system for energy stabilization of distribution network', *Electr. Power Qual. Utilisation*, 2009, **15**, (1), pp. 25–32
[34] Halper, M. S., Ellenbogen, J. C.: 'Supercapacitors: a brief overview', MITRE Nano-systems Group, March 2006, available at www.mitre.org
[35] James, S., Kularatna, N., Ross, A., *et al.*: 'Estimation of transient surgy energy transferred with associated time delays for individual components of surge protector circuits', *Inst. Eng. Technol., IET Power Electron. J.*, 2015, **8**, (5), pp. 685–692
[36] Kumar, M., Reddy, M.: 'Renewable power generation units through micro grid system', *Int. J. Eng. Res. Appl., IJERA*, 2013, **3**, (5), pp. 1559–1563
[37] Ahshan, R., Iqbal, M., Mann, G., *et al.*: 'Modeling and analysis of a microgrid system powered by renewable energy sources', *Open Renew. Energy J.*, 2013, **6**, pp. 7–22
[38] La Seta, I. P.: 'Modeling and control of wind turbines based on doubly-fed induction generators (DFIG)'. EEUG Meeting 2009, TU Delft, the Netherlands, 2009
[39] Wu, F., Zhang, X., Godfrey, K., *et al.*: 'Small signal stability analysis and optimal control of a wind turbine with doubly fed induction generator', *IET Gener. Transm. Distrib.*, 2007, **1**, (5), pp. 751–760
[40] Moura, F., Camacho, J., Resende, J., *et al.*: 'Synchronous generator, excitation and speed governor modeling in ATP-EMTP for interconnected DG studies'. Int. Conf. Electrical Machines, ICEM'08, Vilamoura, Portugal, 2008
[41] Chiesa, N., Høidalen, H. K., Mork, B., *et al.*: 'Implementation and verification of the hybrid transformer model in ATPDraw'. Int. Conf. Power Systems Transients, IPST'07, Lyon, France, 4–7 June 2007
[42] Hassan, E.O., Badran, E.A., Youssef, F.M.H.: 'A comparison between some currently used high frequency transformer models', *Mansoura Eng. J.*, 2013, **39**, (1), pp. E1–E7
[43] Prikler, L., Høidalen, H.: 'ATPDRAW version 5.6 Users' Manual', November 2009
[44] Ali, S. A.: 'Study of short-circuit currents around detmarovice power station', *Trans. Electr. Electron. Mater.*, 2014, **15**, (3), pp. 117–124